Performing Hong-Ou-Mandel-type numerical experiments with repulsive condensates: The case of dark and dark-bright solitons

Zhi-Yuan Sun, Panayotis G. Kevrekidis, and Peter Krüger

Phys. Rev. A **94**, 063645 — Published 28 December 2016

DOI: 10.1103/PhysRevA.94.063645

Performing Hong-Ou-Mandel-type Numerical Experiments with Repulsive Condensates: The case of Dark and Dark-bright Solitons

Zhi-Yuan Sun*
Department of Physics,
Technion-Israel Institute of Technology, Haifa, 32000, Israel

Panayotis G. Kevrekidis
Department of Mathematics and Statistics,
University of Massachusetts, Amherst, MA, USA

Peter Krüger
Midlands Ultracold Atom Research Centre, School of Physics & Astronomy,
The University of Nottingham, Nottingham, UK

(November 13, 2016)

Abstract

The Hong-Ou-Mandel experiment leads indistinguishable photons simultaneously reaching a 50:50 beam splitter to emerge on the same port through two-photon interference. Motivated by this phenomenon, we consider numerical experiments of the same flavor for classical, *wave* objects in the setting of repulsive condensates. We examine dark solitons interacting with a repulsive barrier, a case in which we find no significant asymmetries in the emerging waves after the collision, presumably due to their topological nature. We also consider case examples of two-component systems, where the dark solitons trap a bright structure in the second-component (dark-bright solitary waves). For these, pronounced asymmetries upon collision *are* possible for the non-topological bright component. We also show an example of a similar phenomenology for ring dark-bright structures in two dimensions.

*sunzhiyuan137@aliyun.com Current address: Ministry-of-Education Key Laboratory of Fluid Mechanics and National Laboratory for Computational Fluid Dynamics, Beijing University of Aeronautics and Astronautics (Beihang University), Beijing 100191, China

1 Introduction

The well-known Hong-Ou-Mandel (HOM) effect in quantum mechanics describes particle interference of two indistinguishable photons [1]: when two identical single-photon wave packets simultaneously enter a 50:50 beam splitter, one in each input port, both always exit the splitter at the same output port, although each photon has (on its own) a 50:50 possibility to exit either output port. With this effect, we can test (by the manner of the so-called HOM dip) the degree of indistinguishability of two incoming photons experimentally. Moreover, the HOM effect has been applied to demonstrate the purity of a solid-state single-photon source [2] and has provided a mechanism for logic gates in linear optical quantum computation [3]. Experimental realizations have also been implemented for larger particle numbers such as three photons impinging on a multiport mixer [4], and for one and two-photon pairs [5]. Multi-photon experiments and the associated generalizations of the Hong-Ou-Mandel effect have been reviewed in [6].

Recent studies have generalized the HOM effect to the interference of massive particles [7–11]. In fact, Bose-Einstein condensates (BECs) at very low temperatures provide a setup for studying an analog to the HOM effect for massive (bosonic) particles, such as atoms. Lewis-Swan and Kheruntsyan realized the HOM effect for massive particles by using a collision of two BECs and a sequence of laser-induced Bragg pulses as the splitter [12]. On the other hand, this has been further explored experimentally in a plasmonic setup using surface plasmon polaritons to interact through a semitransparent Bragg mirror [13]. In its most recent implementations, a variant of the HOM experiment involving atoms rather than photons was realized in [14] and another one in the frequency domain involving photons of different colors was achieved in [15]. The latter led to the observation of a pair of photons of the same color at the output of the frequency-domain beam-splitter.

Considering the more *classical* aspect of matter waves, solitary waves or solitons have been extensively studied in the context of BECs; for a recent review, see, e.g., [16]. Bright solitary waves for attractive interactions have been created in ^{7}Li [17, 18] and ^{85}Rb [19], and their interactions (also with barriers) have been explored both at the mean-field and at the quantum-mechanical level [20–26]. At the junction of the HOM effect and matter-wave solitons, we previously have proposed a mean-field analogue of the HOM effect with bright solitons in BECs [27]. In our setup, the bright solitons play the role of a classical wave analogue to the quantum photons, while the role of the beam splitter is played by a repulsive Gaussian barrier. Although these are not quantum mechanical objects at the level of consideration of [27], our analysis showed that their wave character is responsible for an intriguing phenomenology. In particular, we showed that even very slight deviations of the bright solitons from perfect symmetry (of the order of a few percent in the relative speed, or in the relative amplitude) yield an output whereby the bright solitons emerge essentially in only one of the two ports. This feature is demonstrated to be generic in a wide regime of soliton and barrier parameters.

It is then natural to inquire whether similar phenomena may be present in the context of repulsive BECs. While the work of [12] considered this possibility between two BECs, here we consider it at the level of topological wave excitations existing within the (same) BEC.

In particular, we consider the potential of HOM phenomenology with dark (single or multi-component) solitons. Dark matter-wave solitons, which are characterized by localized dips in the atomic density with certain phase slip across their center, have received considerable research interest in atomic systems in recent years [16, 28]. In BECs they can be created by phase imprinting [29–31], destructive interference [32, 33], density engineering [34], and by dragging a potential barrier through the condensate [35–37], among others. Collisions of DSs in an elongated BEC have been observed experimentally [32, 33, 38], showing their potential non-destructive transmission or reflection with a shift in their trajectories. However, it is important to caution here about the necessity for the quasi-one-dimensional nature of the associated geometry, as under less restrictive trapping conditions, different types of collisional effects may arise [39]. On the other hand, interactions of the DSs with localized impurities have been considered in the literature [40, 41], with relevant investigations proposed also in the context of BECs [42–45]. Moreover, such issues on soliton-impurity interactions have been extended to dark-bright (DB) solitons [46, 47], ring dark solitons [48], and vortices [49, 50]. While ring dark solitons have yet to be observed as stable objects experimentally, despite theoretical proposals for their stabilization [51], DB structures have been a focus of considerable experimental interest, as is evidenced by a relevant recent review [52].

In our numerical experiments reported here, we start from dark solitons in repulsive BECs (within the mean-field description of the quasi-1D Gross-Pitaevskii (GP) equation with repulsive interactions), and arrange systematic simulations for the collisions between dark-soliton pair and impurity. Unlike the bright solitons, we find that scattering of the dark-soliton pair (with slight asymmetry) by the impurity is not able to effectively yield the strongly asymmetric behavior reminiscent of the HOM effect. Thus, we further pay attention to the DB solitons in a two-component BEC, with the localized Gaussian impurity (either repulsive or attractive) added on the bright-soliton component. In such a case, systematic simulations show that the dark-soliton component presents an analog of the HOM effect generically. Finally, we give a prototypical case example of analogous behavior in a 2D setup for the ring DB solitons [53].

2 Scattering of dark-soliton pair by impurity

Firstly, we examine the collision phenomenology in the setting of the normalized quasi-1D GP equation with repulsive interactions:

$$i\frac{\partial\psi(x,t)}{\partial t}=\left[-\frac{1}{2}\frac{\partial^2}{\partial x^2}+|\psi(x,t)|^2+\frac{q}{\sqrt{2\pi}\sigma}e^{-\frac{x^2}{2\sigma^2}}\right]\psi(x,t)\ , \tag{1}$$

where $\psi(x,t)$ is the dimensionless wave function with normalized temporal and spatial coordinates t and x, and the Gaussian barrier has a normalized width σ and strength q. Derivation of the dimensionless form of this equation, and discussion of the relevant physical units can be seen, e.g., in [16, 21, 42]. Here, we simply mention that typically the density is measured in units of $(2a)^{-1}$, the spatial extent is measured in units of $\sqrt{\hbar/(m\Omega)}$, time in units of Ω^{-1} and energy in units of $\hbar\Omega$. Ω here plays the role of the transverse confinement frequency, which is effectively tunable in our setting (in the absence of longitudinal confinement).

By a procedure similar to [42, 54], we firstly calculate the profile of the background field with impurity, $\psi(x,t) = \psi_b(x)e^{-i\psi_0^2 t}$, where ψ_0^2 is the normalized density of the BEC cloud:

$$\psi_b(x) \approx \psi_0 - \frac{q}{4}e^{2\sigma^2\psi_0^2}\left[e^{-2\psi_0 x}\mathrm{erfc}\left(\frac{-x+2\sigma^2\psi_0}{\sqrt{2}\sigma}\right) + e^{2\psi_0 x}\mathrm{erfc}\left(\frac{x+2\sigma^2\psi_0}{\sqrt{2}\sigma}\right)\right] , \tag{2}$$

with the assumption that the impurity is small, where $\mathrm{erfc}(z) = 1 - \frac{2}{\sqrt{\pi}}\int_0^z e^{-\eta^2}d\eta$ gives the complementary error function. The background field density $\psi_b^2(x)$ describes an effective background condensate wave function modified by the localized impurity. Dynamics of a single dark soliton on top of such a background with impurity can be approximately described by an adiabatic perturbation, which is briefly summarized in the appendix.

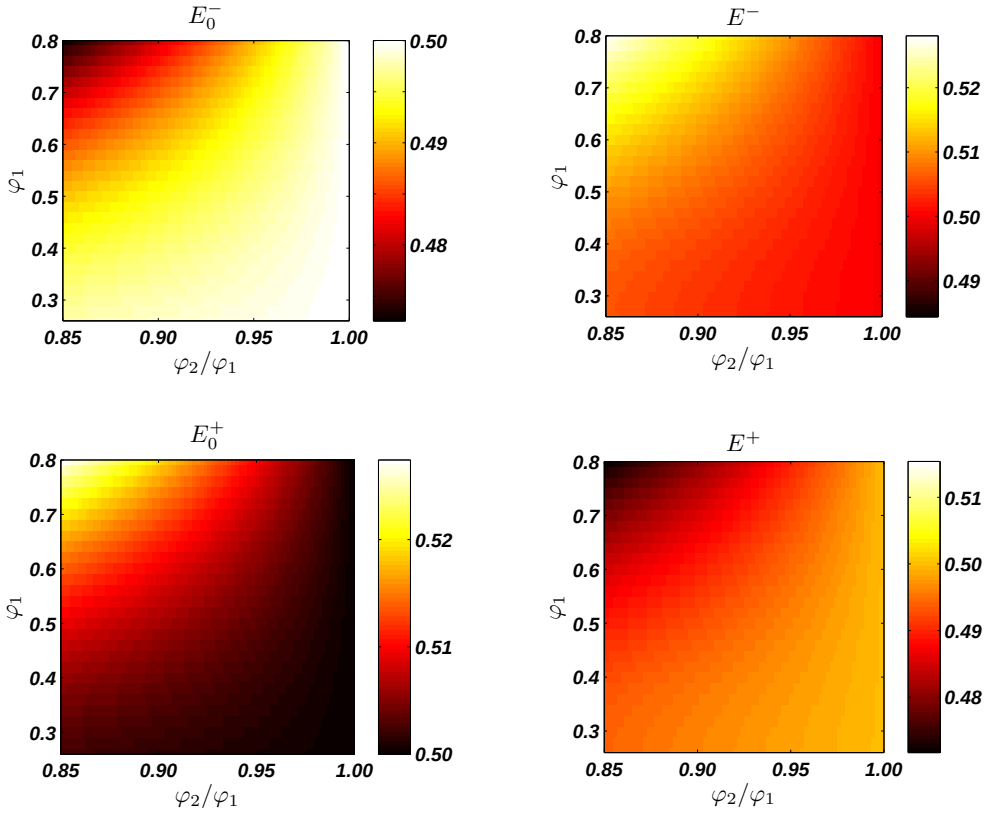

Figure 1: Phase diagram of $E^{\pm}$ before (the left two panels for $t = 0$) and after (the right two panels for $t = 1.6x_1/\sin\varphi_1$) collision. The relevant parameters are $q = 0.3$, $\sigma = 0.1$, $\psi_0 = 1$, and $x_1 = 15$.

For scattering of a dark-soliton pair with small asymmetry, we perform direct simulations of Eq. (1) using a fourth-order Runge-Kutta algorithm in time, and fourth-order centered difference in space scheme. Our initial condition involves two oppositely moving dark solitons that collide at the center of the impurity, with the form,

$$\psi(x,0) = \psi_b(x)\{\cos\varphi_1 \tanh[\cos\varphi_1(x+x_1)] + i\sin\varphi_1\}\{\cos\varphi_2 \tanh[\cos\varphi_2(x-x_2)] - i\sin\varphi_2\} , \tag{3}$$

where $0 \le \varphi_{1,2} < \pi/2$, $x_{1,2} > 0$, and $x_1/x_2 = \sin\varphi_1/\sin\varphi_2$. For sufficiently large values of x_1 and x_2, Eq. (3) approximately represents a pair of two dark solitons located at $-x_1$ and x_2, with

oppositely moving velocities $\sin\varphi_1$ and $-\sin\varphi_2$. The above condition for x_1/x_2 then ensures that the solitons arrive at the the center of the impurity concurrently. In our setup, we control a small difference between φ_1 and φ_2, ensuring that $|(\varphi_2-\varphi_1)/\varphi_1| \leqslant 0.15$. Two normalized integral quantities on each side of the barrier are computed in the numerical experiments[1]

$$E^-(t) = \frac{\int_{-\infty}^{0}(\psi_b^2-|\psi|^2)dx}{\int_{-\infty}^{+\infty}(\psi_b^2-|\psi|^2)dx} \qquad E^+(t) = \frac{\int_{0}^{+\infty}(\psi_b^2-|\psi|^2)dx}{\int_{-\infty}^{+\infty}(\psi_b^2-|\psi|^2)dx}\,. \tag{4}$$

It is easily understood by symmetry that for $\varphi_1=\varphi_2$ and other parameters chosen the same for both incoming dark solitons, we obviously obtain $E^-=E^+=0.5$ after collision. We now consider the case with small asymmetry, and compute a phase diagram of $E^\pm$ after collision for both slow and fast solitons. In the simulation, we control $|E_0^\pm-0.5|\leqslant 0.03$ [$E^\pm(t=0)$ is denoted by $E_0^\pm$] in order to satisfy the small difference between the normalized masses of the two incoming dark solitons; the results are presented in Fig. 1.

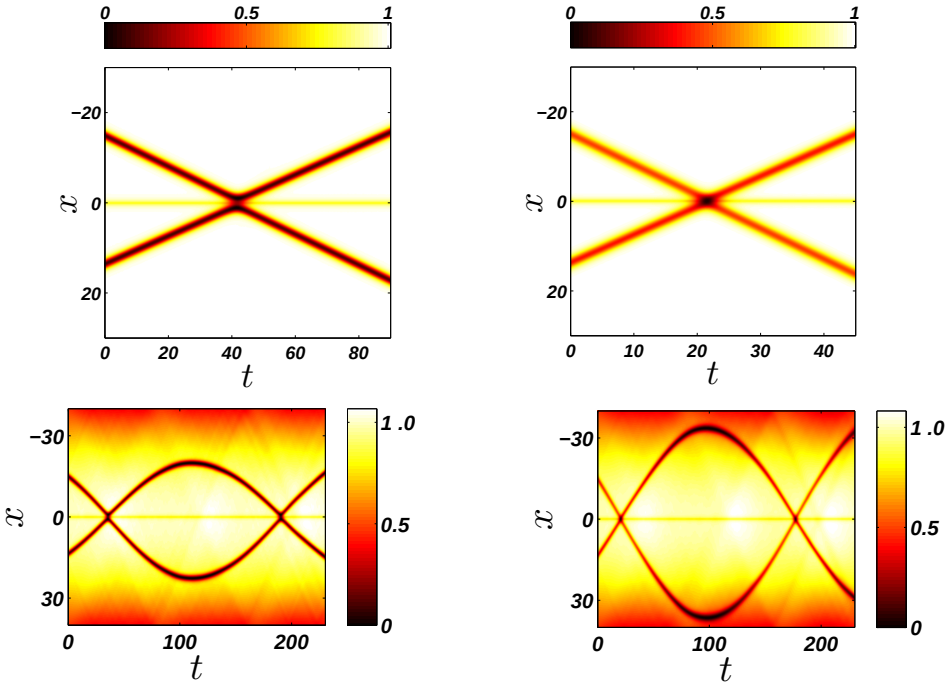

Figure 2: Numerical simulation of a two-dark-soliton collision at center of the impurity. The relevant parameters are $q=0.3$, $\sigma=0.1$, $\mu=1$, $x_1=15$, and $\varphi_2/\varphi_1=0.90$. (a) $\varphi_1=0.35$; (b) $\varphi_1=0.75$; recall that the speed of the first soliton is $\propto\sin(\phi_1)$; (c) $\varphi_1=0.35$ with a parabolic trapping potential $U_{\rm tr}=\frac{1}{2}\Omega^2x^2$ of $\Omega=0.03$; (d) $\varphi_1=0.75$ with $\Omega=0.03$.

From this phase diagram, we see that slight initial differences cannot generate amplified asymmetry in the output. In fact, the basic behavior hereby is simultaneous reflection (transmission) of the two incoming solitons by (through) the Gaussian barrier. Two typical examples

[1]It should be noted that a collision of dark soliton(s) with the barrier always results in pairwise emission of much smaller dark and anti-dark entities on each side. For the anti-dark entity, the integration $\int(\psi_b^2-|\psi|^2)dx<0$, and, the emission of such a negative portion may affect the mass redistribution within the left and right portions of the domain. We verified that this effect had no significant bearing on the reported results.

are shown in Fig. 2, where the left panel is for simultaneous reflection, while the right panel is for simultaneous transmission. Recalling that the speed of the first soliton is $\propto \sin(\phi_1)$, we infer that the left panel corresponds to a slow soliton collision, while the right panel to a fast one, yet the mass distribution between the regions $x < 0$ and $x > 0$ does not change significantly, upon the collision event, among the two cases. We vary the parameters for the repulsive impurity (q and σ), background (ψ_0), and initial soliton position (x_1) in the numerical simulation and the results retain features similar to the one shown above. Additionally, when the conventional parabolic trapping potential $U_{\rm tr}(x) = \frac{1}{2}\Omega^2 x^2$ is introduced, the general features of the phase diagram in Fig. 1 do not change, with two typical examples shown in Figs. 2(c) and (d). On the other hand, for an attractive impurity ($q < 0$), the dark soliton (pair) can generally pass through the barrier, being unable to cause the HOM-analog asymmetry. A particular case occurs for a pair of slow solitons with slight asymmetry: after the collision, one soliton is trapped by the barrier for a short while before it is released to either side of the barrier. However, such an atypical situation is not included in our analogue.

3 Scattering of DB-soliton pairs by impurity

Given the limited ability of dark solitons to feature HOM type extrema in transmission/reflection, which can possibly be partially attributed to their topological character (associated with a phase slip), we now turn to composite structures featuring a non-topological (bright) component, namely to dark-bright solitary waves. An associated physical system can for example be composed of two different hyperfine states of the same alkali isotope [52]. If this condensate is confined in a highly anisotropic trap, with the longitudinal frequency much smaller than the transverse frequency, the mean-field dynamics of the BEC can be described by the following dimensionless system of two coupled GP equations,

$$i\frac{\partial\psi_D(x,t)}{\partial t} = -\frac{1}{2}\frac{\partial^2\psi_D(x,t)}{\partial x^2} + (|\psi_D(x,t)|^2 + g_{12}|\psi_B(x,t)|^2)\psi_D(x,t) + V_D(x)\psi_D(x,t)\ , \tag{5a}$$

$$i\frac{\partial\psi_B(x,t)}{\partial t} = -\frac{1}{2}\frac{\partial^2\psi_B(x,t)}{\partial x^2} + (g_{12}|\psi_D(x,t)|^2 + |\psi_B(x,t)|^2)\psi_B(x,t) + V_B(x)\psi_B(x,t)\ . \tag{5b}$$

Scaling of Eqs. (5) and the relevant physical units can be found in [46, 47]. Upon the choice of the inter-component nonlinearity strength $g_{12} = 1$, the (ratio of) nonlinearity coefficients is taken to be unity, which leads the system of Eqs. (5) to a variant of the well-known Manakov model [55]. Such an assumption is consistent with experiments based on two different hyperfine states of ^{87}Rb [56–59], where the scattering lengths characterizing the intra- and inter-component atomic collisions are almost equal[2]. In what follows, we will also briefly touch upon the immiscible

[2]It should be borne in mind that slight deviations from the limit especially towards the immiscible side may be responsible for fundamentally different dynamical evolutions involving phase separation between the components [56]. Yet, DB solitons have been identified as existing on both sides of this transition [60].

(between the two components) regime of $g_{12} > 1$. For simplicity, though, it should be assumed that $g_{12} = 1$, except where specified otherwise. On the other hand, $V_{D,B}(x)$ represent the normalized external potentials; in our setup, we consider a localized Gaussian potential (impurity) added in the component 2 that supports a bright soliton, namely $V_B(x) = \frac{q}{\sqrt{2\pi}\sigma} e^{-\frac{x^2}{2\sigma^2}}$ and $V_D(x) = 0$. The potential can be generated by off-resonant Gaussian laser beams, and for a blue- or red-detuned laser beam, the impurity potential can either repel ($q > 0$) or attract ($q < 0$) the atoms of the relevant component of the condensate.

For our analog of the HOM phenomenology, the Gaussian impurity plays the role of the splitter, and the DB-soliton pairs with slight asymmetry play the role of photons. With the boundary conditions $|\psi_D|^2 \to \mu$ and $|\psi_B|^2 \to 0$ as $|x| \to \infty$, the incoming soliton pairs (the initial conditions in the simulation) are chosen as the following form that describes two DB solitons colliding at the center of the impurity:

$$\psi_D(x,0) = \sqrt{\mu}\{\cos\alpha_1 \tanh[k_1(x+x_1)] + i\sin\alpha_1\}\{\cos\alpha_2 \tanh[k_2(x-x_2)] - i\sin\alpha_2\} \ , \tag{6a}$$

$$\psi_B(x,0) = A_1 \mathrm{sech}[k_1(x+x_1)]e^{iv_1 x} + A_2 \mathrm{sech}[k_2(x-x_2)]e^{-i(v_2 x+\Delta)} \ , \tag{6b}$$

where α_j is the dark soliton's phase angle, $\sqrt{\mu}\cos\alpha_j$ and A_j are the amplitudes of the dark and bright solitons, k_j and $(-1)^j x_j$ are associated with the inverse width and the initial position of the DB solitons, and $(-1)^{j-1}v_j$ and Δ represent the soliton velocity and a relative phase. These parameters of the DB-soliton pairs satisfy the following relations:

$$k_j^2 + A_j^2 = \mu\cos^2\alpha_j \ , \tag{7a}$$

$$v_j = k_j \tan\alpha_j \quad (j = 1, 2), \tag{7b}$$

$$x_1/v_1 = x_2/v_2 \ . \tag{7c}$$

In our analogue, we choose two independent parameters k_j and v_j, and consider nontrivial deviations between the parameters of the two DB solitons. In this case, there are two sets of masses, respectively, for the dark and bright components in order to quantify relevant transfer.

$$E_B^-(t) = \frac{\int_{-\infty}^{0}|\psi_B|^2 dx}{\int_{-\infty}^{+\infty}|\psi_B|^2 dx} \qquad E_B^+(t) = \frac{\int_{0}^{+\infty}|\psi_B|^2 dx}{\int_{-\infty}^{+\infty}|\psi_B|^2 dx} \ , \tag{8a}$$

$$E_D^-(t) = \frac{\int_{-\infty}^{0}(\mu - |\psi_D|^2) dx}{\int_{-\infty}^{+\infty}(\mu - |\psi_D|^2) dx} \qquad E_D^+(t) = \frac{\int_{0}^{+\infty}(\mu - |\psi_D|^2) dx}{\int_{-\infty}^{+\infty}(\mu - |\psi_D|^2) dx}. \tag{8b}$$

We prescribe these normalized masses to feature small deviations from symmetry (with $|E_{B,D}^{\pm}(0) - 0.5| \leqslant 0.03$ in general). The simulation results will be systematically presented below

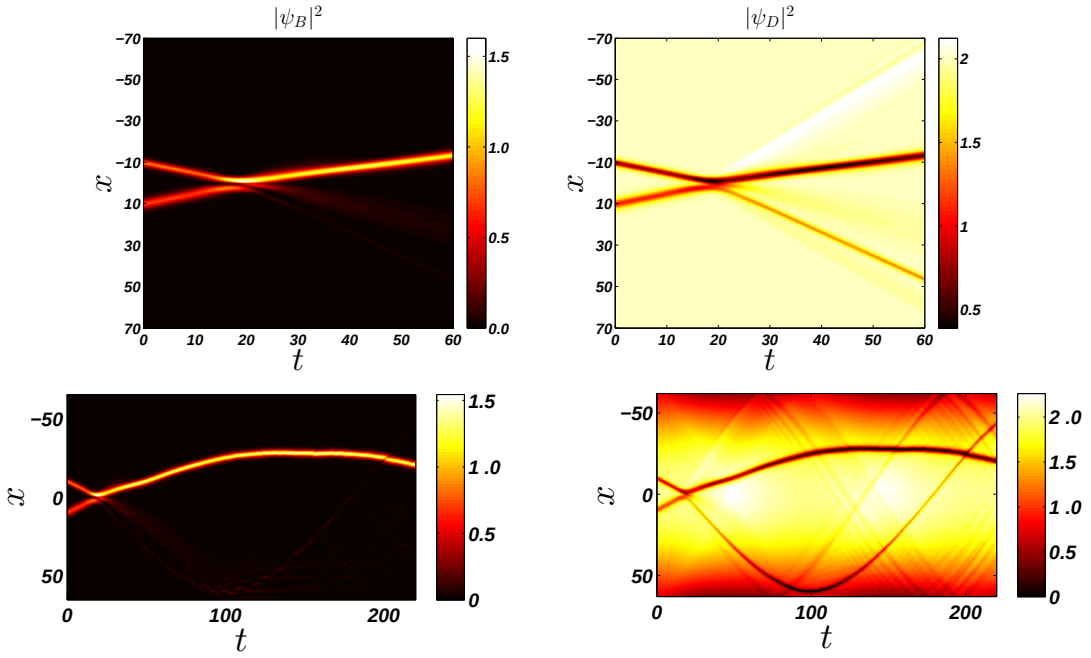

Figure 3: Numerical simulation of a two-DB-soliton collision at the center of impurity. The relevant parameters are $q = 1$, $\sigma = 0.1$, $\mu = 2$, $k_1 = 0.66$, $k_2 = 0.46$, $v_1 = v_2 = 0.5$, $x_1 = 10$, and $\Delta = 0$. The lower two panels show the collision with a parabolic trapping potential $U_{\rm tr} = \frac{1}{2}\Omega^2 x^2$ of $\Omega = 0.03$.

Firstly, we consider the case of unequal inverse widths, and illustrate typical realizations in Fig. 3. With the parameters in this figure, the difference in the inverse widths directly leads to a very slight asymmetry of $E_D^{\pm}(0)$ (that is $|E_D^{\pm}(0) - 0.5| \lesssim 1.5\%$), which, after collision at the impurity, induces a much larger deviation on the normalized masses ($E_D^{-} \approx 60\%$). The lower two panels in this figure also illustrate the collision upon the addition of a trapping potential, which shows that the general feature does not change. It is relevant to mention here a feature that can be observed in this case in the dark component which was absent, e.g., in Fig. 2. In particular, for $x < 0$, a white "jet" can be discerned past the collision time in this component. From the colorbar, we can infer that this is a bright solitary wave *on top of the finite background*, hence a structure that is referred to as an anti-dark soliton. Similar structures have not only been discussed in atomic BECs [61], but possible experimental realizations [62], including a recent successful manifestation thereof [63], have been presented.

Figure 4 examines the role of the difference between k_1 and k_2 by fixing k_1, and varying k_2 in the range of $0.6 - 1.0$ (ensuring $|E_D^{\pm}(0) - 0.5| \lesssim 3.0\%$), with the results $E_{B,D}^{-}$ (after collision) shown in this figure. We see that a peak value occurs for both $E_{B,D}^{-}$ when k_2/k_1 varies in the range, which means more of the soliton mass (or the normalized mass) is found on one side. We observe that such a maximum asymmetry for the bright (non-topological) component is considerably stronger than that for the dark component. On the other hand, the situation is almost symmetric as k_2/k_1 varies from 1 to higher values (not shown here). For completeness, Fig. 5 shows the variation upon adding a parabolic trapping potential, also for an immiscible case of $g_{12} = 1.1$. Equation (8a) is still valid when $\Omega \neq 0$, and Fig. 5(a) shows the trapping

potential would not change the asymmetric output. On the other hand, a typical example of the immiscibility ($g_{12} = 1.1$) is presented in Fig. 5(b), indicating that HOM-type collision of the DB solitons is possible up to the immiscible regime.

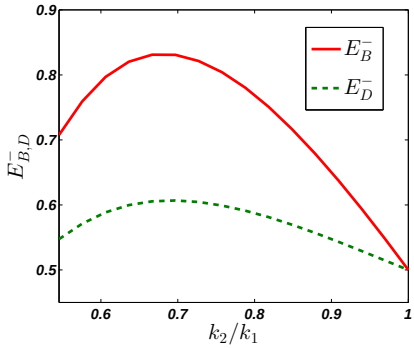

Figure 4: Plots of $E_{B,D}^-$ as a function of k_2/k_1 varying from 0.6 to 1.0 ($k_1 = 0.66$). The relevant parameters are $q = 1$, $\sigma = 0.1$, $\mu = 2$, $v_1 = v_2 = 0.5$, $x_1 = 10$, and $\Delta = 0$.

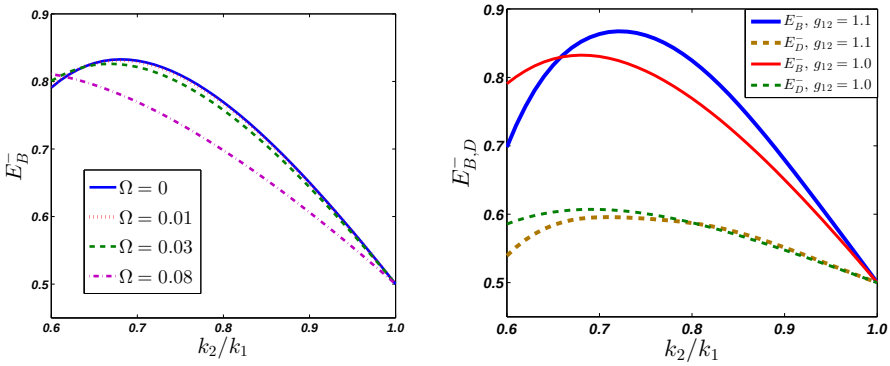

Figure 5: Plots of $E_{B,D}^-$ as a function of k_2/k_1 varying from 0.6 to 1.0 ($k_1 = 0.66$). The relevant parameters are $q = 1$, $\sigma = 0.1$, $\mu = 2$, $v_1 = v_2 = 0.5$, $x_1 = 10$, and $\Delta = 0$. Left panel: $\Omega = 0$, 0.01, 0.03, and 0.08, respectively (note that the curves for $\Omega = 0$ and $\Omega = 0.01$ almost overlap); Right panel: comparison between the miscible ($g_{12} = 1.0$) and immiscible ($g_{12} = 1.1$) examples.

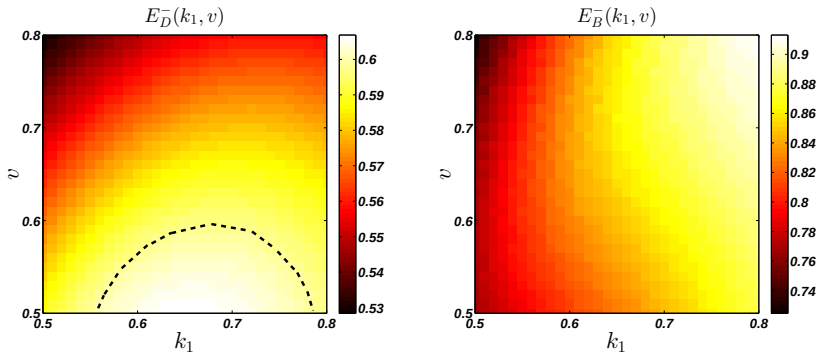

Figure 6: Two-parameter diagram of the propagation asymmetry for the dark (left) and bright (right) components of the DB solitons. The relevant parameters are $q = 1$, $\sigma = 0.1$, $\mu = 2$, $x_1 = 10$, and $\Delta = 0$.

To further check the dependence of the maximum asymmetry with k_1 and v ($v_1 = v_2 = v$), a phase diagram is presented in Fig. 6, where fixing each group of (k_1, v), we vary the value of k_2/k_1, and capture the maximum asymmetry of both $E^-_{B,D}$. It can be seen that features reminiscent of the HOM asymmetry are clearly evident for the slow solitons with k_1 varying in the range $0.55 - 0.75$ (the corresponding suitable regime is within the dashed line in the figure). The maximum asymmetry with $E^-_D \approx 60\%$ is induced by much smaller initial deviation $|E^\pm_D(0) - 0.5| \lesssim 1.5\%$. However, the phenomenology is fundamentally more pronounced in the bright component where it is clear that a behavior reminiscent of the HOM effect can be classically observed for these non-topological waves with E^-_B exceeding values of 0.9. A case example of this is shown in Fig. 3.

Another interesting possibility is to explore the behavior of the DB solitons for an attractive impurity ($q < 0$). We firstly discuss the case where an asymmetry is induced between k_1 and k_2 (for typical parameters, we control k_2/k_1 varying in the range of $0.8 - 1.0$, keeping $|E^\pm_D(0) - 0.5| \lesssim 3.0\%$). For $q < 0$, a very slight portion of soliton mass (normalized mass) is trapped by the impurity after the collision. This hardly influences the phenomenology, and the integration boundary in (8) can be carefully selected[3]. We study the dependence of $E^-_{B,D}$ as k_2/k_1 varies from 0.8 to 1.0, with two groups of results provided in Fig. 7 (two fixed values of k_1 are chosen). We see that generally for the dark (component) solitons the asymmetric output is more pronounced with small velocity. Again, these asymmetries are much stronger in the non-topological component carrying the bright structure, rather than in the topological dark solitons.

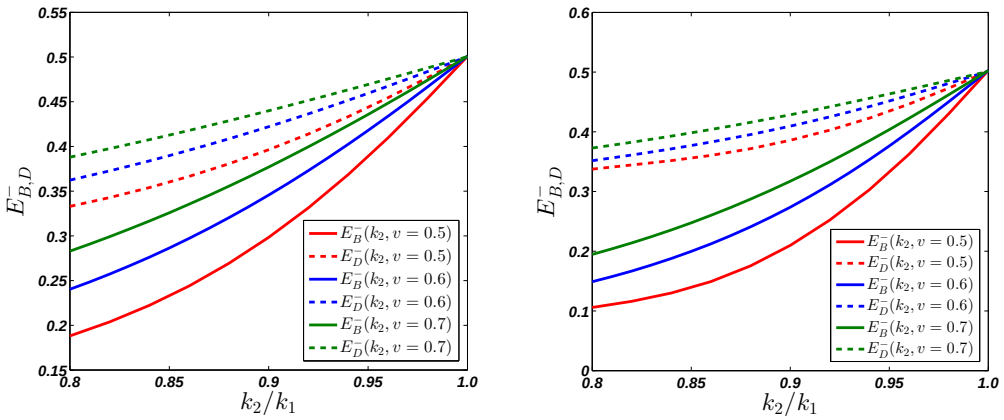

Figure 7: Plots of $E^-_{B,D}$ as a function of k_2/k_1 varying from 0.8 to 1.0 ($k_1 = 0.40$ for the left panel, and $k_1 = 0.50$ for the right panel). The relevant parameters are $q = -1$, $\sigma = 0.1$, $\mu = 2$, $x_1 = 10$, and $\Delta = 0$. These solid and dashed lines in both figures, from upper to lower, correspond to the values of v of 0.7, 0.6, and 0.5, respectively.

A variation of the subject is that deviations in soliton velocities may also induce an asymmetry of the collisional output. Since the deviation $|E^\pm_D(0) - 0.5|$ markedly increases with

[3]For instance, the integration can be revised as $\int_{-\infty}^{0} \to \int_{-\infty}^{-\sigma}$ and $\int_{0}^{+\infty} \to \int_{\sigma}^{+\infty}$ for this situation.

increasing difference between v_1 and v_2 (setting $k_1 = k_2 = k$), we control $|E_D^{\pm}(0) - 0.5| \lesssim 3.0\%$ in our simulations. In this situation the function $E_{B,D}^{-}$ varies with v_2/v_1 (v_1 is fixed) is similar to that of Fig. 7. Therefore, we capture the maximum asymmetry, and draw a two-parameter diagram for the dependence of the corresponding $E_{B,D}^{-}$ on v_1 and k, as shown in Fig. 8. It can be seen that the asymmetric outcome is more pronounced for the fast-moving solitons for both of the dark and bright components, with the bright components, as usual, featuring the most dramatic asymmetry. This feature is partially different from the one of Fig. 6, where the maximum asymmetry tends to occur for the narrower solitons, in particular for the slow dark (component) solitons.

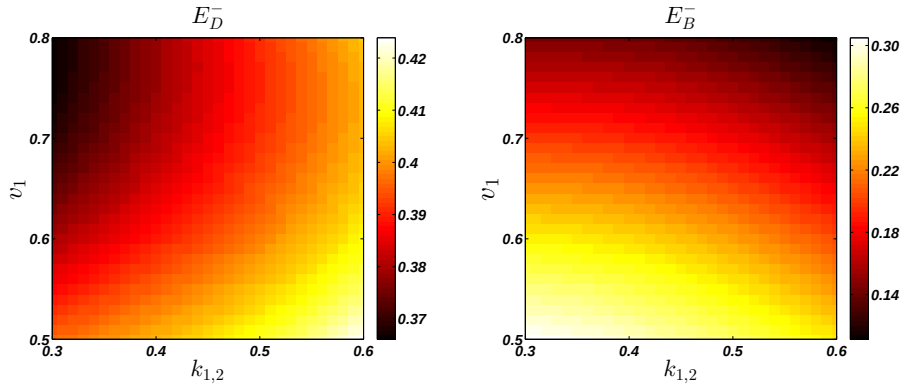

Figure 8: Two-parameter diagram of the maximum asymmetry for the DB solitons, again for dark (left) and bright (right) components. The relevant parameters are $q = 1$, $\sigma = 0.1$, $\mu = 2$, $x_1 = 20$, and $\Delta = 0$.

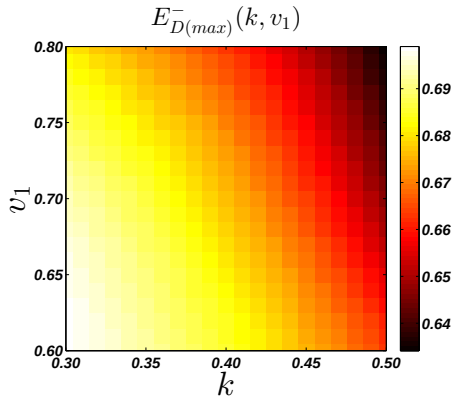

Figure 9: Two-parameter diagram of the asymmetry for the dark solitons (component). The relevant parameters are $q = -1$, $\sigma = 0.1$, $\mu = 2$, $x_1 = 20$, and $\Delta = 0$.

Also, for the attractive impurity, the deviations of soliton velocities can induce maximal asymmetry after the soliton collision. Numerical simulations show that this behavior is captured in a narrow regime of parameters (k, v_1). We study the variation of $E_{B,D}^{-}$ as a function of v_2/v_1 that varies in the range of $0.8 - 1.0$, ensuring $|E_D^{\pm}(0) - 0.5| \lesssim 4.0\%$. The functions are similar to those shown in Fig. 4, with a maximum asymmetry (peak values) as v_2/v_1 varies. In the same way, we draw a phase diagram of the maximum asymmetry for the parameters (k, v_1), as

illustrated in Fig. 9. We observe that the outcome after the collision is more asymmetric for the slower and wider dark (component) solitons.

In addition, we briefly examine the dependence of the asymmetric output on the starting soliton location x_1. We perform simulations with different selections of x_1. The results are presented in Fig. 10. These figures show that the trend of asymmetry is increasing in general as the location x_1 increases. Figures 10(a) and (c) display that the *optimal* point produces a substantial asymmetry ($k_2/k_1 \to 1$ or $v_2/v_1 \to 1$) as x_1 increases. Fig. 10(b) shows that for such type of variation, the asymmetry is generally increasing (k_2/k_1 varies in the whole range of $0.8 - 1.0$) as x_1 is increased.

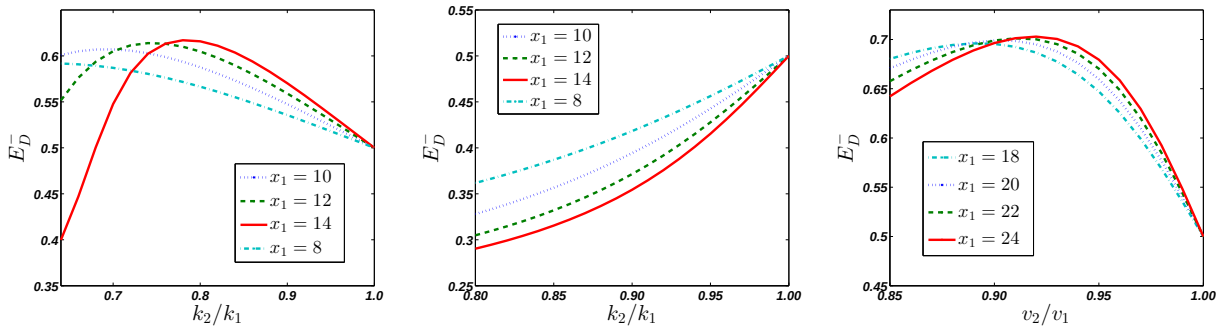

Figure 10: (a) Plots of E_D^- (after collision) as a function of k_2/k_1. The relevant parameters are $q = 1$, $\sigma = 0.1$, $\mu = 2$, $v_1 = v_2 = 0.5$, $k_1 = 0.66$, and $\Delta = 0$. x_1 is equal to 8, 10, 12, and 14, respectively. (b) Plots of E_D^- as a function of k_2/k_1. The relevant parameters are $q = -1$, $\sigma = 0.1$, $\mu = 2$, $v_1 = v_2 = 0.5$, $k_1 = 0.40$, and $\Delta = 0$. x_1 is equal to 8, 10, 12, and 14, respectively. (c) Plots of E_D^- as a function of v_2/v_1. The relevant parameters are $q = -1$, $\sigma = 0.1$, $\mu = 2$, $k_1 = k_2 = 0.3$, $v_1 = 0.60$, and $\Delta = 0$. x_1 is equal to 18, 20, 22, and 24, respectively.

4 Scattering of ring DB-soliton pairs by impurity

In this section, we will briefly extend the asymmetric collision to the 2D case, and illustrate a first example with the ring DB solitons [53]. We consider the evolution of the two-component BEC very near zero temperature governed by the following coupled GP equations with external potential (the two-dimensional Manakov model),

$$i\frac{\partial \psi_D}{\partial t} = -\frac{1}{2}\nabla^2\psi_D + (|\psi_D|^2 + |\psi_B|^2)\psi_D + V_D(r)\psi_D \ , \tag{9a}$$

$$i\frac{\partial \psi_B}{\partial t} = -\frac{1}{2}\nabla^2\psi_B + (|\psi_D|^2 + |\psi_B|^2)\psi_B + V_B(r)\psi_B \ , \tag{9b}$$

where $\nabla^2 = \frac{\partial^2}{\partial x^2} + \frac{\partial^2}{\partial y^2}$ and $r^2 = x^2 + y^2$. In order to study the asymmetric interaction of a ring DB-soliton pair with a localized ring-shaped impurity, we set the external potentials as

$$V_D(r) = 0 \ , \quad V_B(r) = \frac{q}{\sqrt{2\pi}\sigma} e^{-\frac{(r-r_0)^2}{2\sigma^2}} \ , \tag{10}$$

where the ring impurity is localized at $r = r_0$. In simulations, the initial condition used to integrate Eqs. (9) has the same form as (6), whereby $k_j(x - x_j)$ is replaced by $k_j(r - r_j)$, in which r_j is the initial ring soliton radius, and relations of other parameters are similar to (6) and (7). We demonstrate a realization in Fig. 11, where the ring DB-soliton pairs collide at time $t \approx 10$. It can be seen that the asymmetric outcome after collision is still valid for the 2D ring DB solitons. In particular, in this example the inner ring ends up carrying the majority of the relevant non-topological component mass, while the outer one is nearly "extinct" in its bright component. This serves to illustrate that there should be intriguing analogies to the HOM-type phenomenology in higher dimensions, including possibly ones involving vorticity-bearing structures, that are worth exploring and comparing/contrasting with the one-dimensional case.

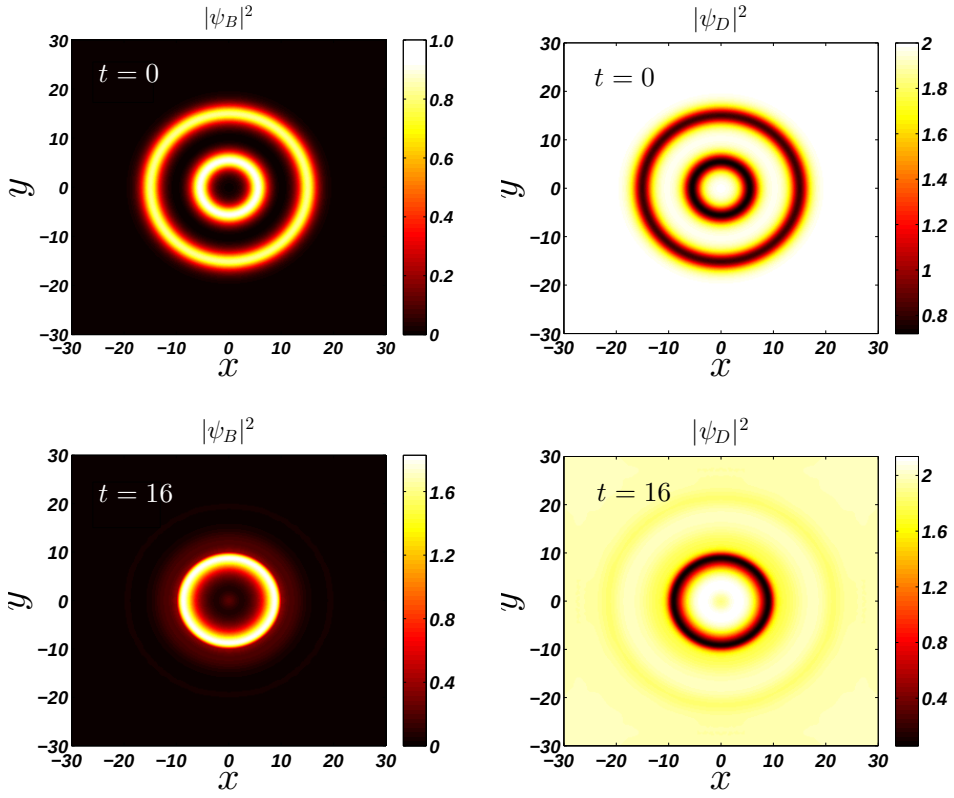

Figure 11: Numerical simulation of a ring DB soliton collision at the center of the ring-shaped impurity. The relevant parameters are $q = 1$, $\sigma = 0.1$, $\mu = 2$, $k_1 = k_2 = 0.60$, $v_1 = 0.50$, $v_2 = 0.45$, $r_1 = 5$, $r_0 = 10$, and $\Delta = 0$.

5 Conclusions and Future Challenges

In the present work we explored the phenomenology of a classical wave analogue motivated by the Hong-Ou-Mandel effect. Instead of using photons and their quantum interference with a beam splitter, we considered wave-like excitations in a repulsive bosonic gas described at the mean-field level by a Gross-Pitaevskii equation. The waves (the interfering entities) were either dark solitons or dark-bright solitons. The role of the beam splitter was played by an

external Gaussian beam. Contrary to our earlier findings for the potential of bright solitons to exhibit very sensitive interference patterns reminiscent of the HOM effect, dark solitons seemed far less efficient in exhibiting such an effect. This may arguably be due to their topological character. This, in turn, led us to explore multi-component dark-bright entities where the non-topological component is symbiotic to the topological one, i.e., supported by the dark component as an effective trapping potential to the bright component. In this case, the results were far more promising leading the bright component in one of the waves possibly to nearly complete extinction, depending on the velocity and width parameters of the incoming waves. Finally, a proof-of-principle example was shown for the two-dimensional case of ring dark-bright solitary waves, where the same phenomenology persisted in the presence of the curvature associated with the ring-like excitations.

While this is a first step in this promising direction of research, numerous additional studies emerge as relevant for future work. On the one hand, both for the bright and the dark case a quantitative understanding of the interference phenomenology and how it differs in the presence of a potential from the integrable (simply phase shifting) phenomenology of the integrable cubic nonlinear Schrödinger model would be a crucial contribution to this theme. Arguably, an especially relevant approach to consider in this regard, perhaps first in the single component attractive case of bright solitons and then in the repulsive two-component setting of dark-bright ones is through the use of variational methods [64]. Generally, the theme of higher dimensional explorations that we touch upon here is an especially interesting one. In the bright soliton (focusing or attractive) case, one can envision for example two solitary waves that are subcritical (or close to critical) which upon such a collision may become supercritical in mass and feature collapse rather than their individual tendency towards dispersion. In the repulsive/defocusing nonlinearity scenario, understanding the quantitative details of how curvature affects the picture through ring DB collisions, or how the presence of vortices (and the interaction of vortex-bright solitary waves [52]) modifies the mass redistribution are important steps towards a deeper understanding of the role of dimensionality. In the case of vortices, it does not escape us that their topological nature (coupled to the absence of one parameter families of such solutions for a given background density – contrary to what is the case with dark solitons) suggests very minor mass redistributions in the component bearing the vorticity. However, mass redistribution is certainly possible and relevant to explore in the non-topological component. In the latter, it has been shown to occur even on the basis of stability properties and tunneling phenomena alone, rather than collision-induced exchanges [65]. These questions are currently under consideration and will be reported in future publications.

6 Appendix

To describe a dark soliton on top of the background with impurity, we write the solution of Eq. (1) in the form,

$$\psi(x,t) = \psi_b(x) e^{-i\psi_0^2 t} \phi(x,t) \ , \tag{11}$$

with $\phi(x,t)$ chosen as

$$\phi(x,t) = \cos(\varphi)\tanh[\cos(\varphi)(x-x_0)] + i\sin(\varphi)\ , \tag{12}$$

where φ is a slowly varying function of t, and $x_0 = \int_0^t \sin(\varphi)d\tau$. Following the adiabatic perturbation approach [42, 54], $\phi(x,t)$ satisfies the following perturbed equation (assume $\psi_0 = 1$ without loss of generality),

$$i\frac{\partial\phi}{\partial t} + \frac{1}{2}\frac{\partial^2\phi}{\partial x^2} - (|\phi|^2 - 1)\phi = P(\phi)\ , \tag{13}$$

where the perturbation $P(\phi)$ has the form

$$P(\phi) = \frac{2H_-(x)}{-4 + H_+(x)}\frac{\partial\phi}{\partial x} - \frac{1}{2}H_+(x)(|\phi|^2 - 1)\phi\ , \tag{14}$$

where

$$H_\pm(x) = qe^{2\sigma^2}\left[e^{-2x}\mathrm{erfc}\left(\frac{-x+2\sigma^2}{\sqrt{2}\sigma}\right) \pm e^{2x}\mathrm{erfc}\left(\frac{x+2\sigma^2}{\sqrt{2}\sigma}\right)\right]\ . \tag{15}$$

As shown in [42, 54], the evolution equation for $\varphi(t)$ can be derived as

$$\frac{\partial\varphi}{\partial t} = \frac{1}{2\cos^2(\varphi)\sin(\varphi)}\mathrm{Re}\left[\int_{-\infty}^{+\infty} P(\phi)\frac{\partial\phi^*}{\partial t}dx\right]\ . \tag{16}$$

Substituting (14) into (16), and assuming φ to be a small quantity [i.e., $\sin(\varphi) \approx \varphi$ and $\cos(\varphi) \approx 1 - \varphi^2/2$], we obtain the following result by neglecting the higher-order terms

$$(1-A)\frac{\partial\varphi}{\partial t} = B\ , \tag{17}$$

where

$$\begin{aligned} A = &\int_{-\infty}^{+\infty}\frac{1}{4}qe^{2\sigma^2}H_+(x)\mathrm{sech}^4(\xi)[1-\xi\tanh(\xi)]dx \\ &+\int_{-\infty}^{+\infty}\frac{\mathrm{sech}^4(\xi)\left[2 - qe^{-2x+2\sigma^2}\mathrm{erfc}\left(\frac{-x+2\sigma^2}{\sqrt{2}\sigma}\right)\right][\sinh(2\xi)+2\xi]}{-4+qe^{2\sigma^2}H_+(x)}dx\ , \end{aligned} \tag{18a}$$

$$\begin{aligned} B = &\int_{-\infty}^{+\infty}\mathrm{sech}^4(\xi)\left[1 - \frac{1}{4}qe^{2\sigma^2}H_+(x)\tanh(\xi)\right]dx \\ &+\int_{-\infty}^{+\infty}\frac{\mathrm{sech}^4(\xi)\left[4 - 2qe^{-2x+2\sigma^2}\mathrm{erfc}\left(\frac{-x+2\sigma^2}{\sqrt{2}\sigma}\right)\right]}{-4+qe^{2\sigma^2}H_+(x)}dx\ , \end{aligned} \tag{18b}$$

where $\xi = x - x_0$. Numerically evaluating the integrals of (18), and considering the effective particle approach for x_0, we can write the effective potential where the soliton center moves in

$$U(x) = -\int_\infty^x \frac{d^2x_0}{dt^2}dx_0 \approx -\int_\infty^x \frac{\partial\varphi}{\partial t}dx_0\ . \tag{19}$$

For the repulsive impurity, we can obtain a critical value φ_c that the effective kinetic energy equals to the height of the effective potential, i.e.,

$$\frac{1}{2}\sin^2(\varphi_c) = U_{max}(x)\ . \tag{20}$$

Theoretically speaking, when $\varphi > \varphi_c$, the dark soliton transmits the impurity barrier; otherwise, when $\varphi < \varphi_c$, the soliton is reflected by the barrier. We perform direct simulations of Eq. (1) (the numerical method is the same as in the main content) to find a sequence of values φ_c, and make a comparison with (20), as shown in Fig. 12. The results accord well when q is small (φ_c is small as well), which is reasonable under the assumption of our effective potential approach.

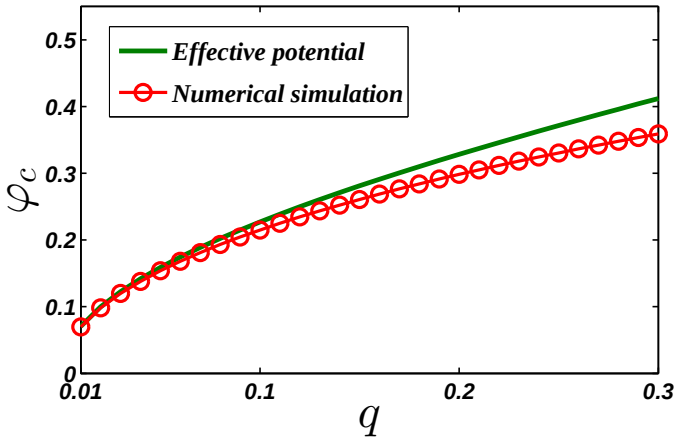

Figure 12: Comparison of φ_c between the effective potential approach (20) and direct simulation of Eq. (1) ($\sigma = 0.1$).

References

[1] C. K. Hong, Z. Y. Ou, and L. Mandel, Phys. Rev. Lett. **59**, 2044 (1987).

[2] C. Santori, D. Fattal, J. Vučković, G. S. Solomon, and Y. Yamamoto, Nature (London) **419**, 594 (2002).

[3] E. Knill, R. Laflamme, and G. J. Milburn, Nature (London) **409**, 46 (2001).

[4] R. Campos. Three-photon hong-ou-mandel interference at a multiport mixer. Phys. Rev. A **62**, 013809 (2000).

[5] O. Cosme, S. Pádua, F. Bovino, A. Mazzei, F. Sciarrino, and F. De Martini. Hong-Ou-mandel interferometer with one and two photon pairs. Phys. Rev. A **77**, 053822 (2008).

[6] Z. Y. Ou. Multi-photon interference and temporal distinguishability of photons. Int. J. Mod. Phys. B **21**, 5033 (2007).

[7] Y. L. Lim and A. Beige, New J. Phys. **7**, 155 (2005).

[8] P. Longo, J. H. Cole, and K. Busch, Opt. Express **20**, 12326 (2012).

[9] F. Laloë and W. J. Mullin, Found. Phys. **42**, 53 (2012).

[10] B. Gertjerenken and P. G. Kevrekidis, Phys. Lett. A **379**, 1737 (2015).

[11] W.J. Mullin and F. Laloë, Phys. Rev. A **91**, 053629 (2015).

[12] R. J. Lewis-Swan and K. V. Kheruntsyan, Nat. Commun. **5**, 3752 (2014).

[13] G. Di Martino, Y. Sonnefraud, M. S. Tame, S. Kéna-Cohen, F. Dieleman, S. K. Özdemir, M. S. Kim, and S. A. Maier, Phys. Rev. Applied **1**, 034004 (2014).

[14] R. Lopes, A. Imanaliev, A. Aspect, M. Cheneau, D. Boiron and C.I. Westbrook, Nature **520**, 66 (2015).

[15] T. Kovayashi, R. Ikuta, S. Yasui, S. Miki, T. Yamashita, H. Terai, T. Yamamoto, M. Koashi, N. Imoto, Nature Phot. **10**, 441 (2016).

[16] P. G. Kevrekidis, D. J. Frantzeskakis, and R. Carretero-González, *Emergent Nonlinear Phenomena in Bose-Einstein Condensates: Theory and Experiment*, Springer Series on Atomic, Optical, and Plasma Physics Vol.45 (Springer, Berlin, 2008).

[17] L. Khaykovich, F. Schreck, G. Ferrari, T. Bourdel, J. Cubizolles, L. D. Carr, Y. Castin, and C. Salomon, Science **296**, 1290 (2002).

[18] K. E. Strecker, G. B. Partridge, A. G. Truscott, and R. G. Hulet, Nature (London) **417**, 150 (2002); New J. Phys. **5**, 73 (2003).

[19] S. L. Cornish, S. T. Thompson, and C. E. Wieman, Phys. Rev. Lett. **96**, 170401 (2006).

[20] T. P. Billam, A. L. Marchant, S. L. Cornish, S. A. Gardiner, and N. G. Parker, *Bright Solitary Matter Waves: Formation, Stability and Interactions in Spontaneous Symmetry Breaking, Self-Trapping, and Josephson Oscillations*, edited by B. A. Malomed, (Springer-Verlag, New York, 2013).

[21] J. L. Helm, T. P. Billam, and S. A. Gardiner, Phys. Rev. A **85**, 053621 (2012).

[22] J. Cuevas, P. G. Kevrekidis, B. A. Malomed, P. Dyke, and R. G. Hulet, New J. Phys. **15**, 063006 (2013).

[23] A. D. Martin and J. Ruostekoski, New J. Phys. **14**, 043040 (2012).

[24] B. Gertjerenken, T. P. Billam, L. Khaykovich, and C. Weiss, Phys. Rev. A **86**, 033608 (2012).

[25] A. L. Marchant, T. P. Billam, T. P. Wiles, M. M. H. Yu, S. A. Gardiner, and S. L. Cornish, Nat. Commun. **4**, 1865 (2013).

[26] J. H. V. Nguyen, P. Dyke, D. Luo, B. A. Malomed, and R. G. Hulet, Nat. Phys. **10**, 918 (2014).

[27] Z.-Y. Sun, P. G. Kevrekidis, and P. Krüger, Phys. Rev. A **90**, 063612 (2014).

[28] D. J. Frantzeskakis, J. Phys. A **43**, 213001 (2010).

[29] S. Burger, K. Bongs, S. Dettmer, W. Ertmer, K. Sengstock, A. Sanpera, G. V. Shlyapnikov, and M. Lewenstein, Phys. Rev. Lett. **83**, 5198 (1999).

[30] J. Denschlag, J. E. Simsarian, D. L. Feder, C. W. Clark, L. A. Collins, L. Cubizolles, J. ans Deng, E. W. Hagley, K. Helmerson, W. P. Reinhardt, S. L. Rolston, B. I. Schneider, and W. D. Phillips, Science **287**, 97 (2000).

[31] C. Becker, S. Stellmer, P. Soltan-Panahi, S. Dörscher, M. Baumert, E.M. Richter, J. Kronjäger, K. Bongs, and K. Sengstock, Nat. Phys. **4**, 496 (2008).

[32] A. Weller, J. P. Ronzheimer, C. Gross, J. Esteve, M. K. Oberthaler, D. J. Frantzeskakis, G. Theocharis, and P. G. Kevrekidis Phys. Rev. Lett. **101**, 130401 (2008).

[33] G. Theocharis, A. Weller, J. P. Ronzheimer, C. Gross, M. K. Oberthaler, P. G. Kevrekidis, and D. J. Frantzeskakis Phys. Rev. A **81**, 063604 (2010).

[34] B. P. Anderson, P. C. Haljan, C. A. Regal, D. L. Feder, L. A. Collins, C. W. Clark, and E. A. Cornell, Phys. Rev. Lett. **86**, 2926 (2001).

[35] N. Pavloff, Phys. Rev. A **66**, 013610 (2002).

[36] P. Engels and C. Atherton, Phys. Rev. Lett. **99**, 160405 (2007).

[37] I. Hans, J. Stockhofe, and P. Schmelcher, Phys. Rev. A **92**, 013627 (2015).

[38] S. Stellmer, C. Becker, P. Soltan-Panahi, E.M. Richter, S. Dörscher, M. Baumert, J. Kronjäger, K. Bongs, and K. Sengstock, Phys. Rev. Lett. **101**, 120406 (2008).

[39] C. Becker, K. Sengstock, P. Schmelcher, P.G. Kevrekidis, R. Carretero-González, New J. Phys. **15**, 113028 (2013).

[40] Yu. S. Kivshar and B. A. Malomed, Rev. Mod. Phys. **61**, 763 (1989).

[41] V. V. Konotop, V. M. Pérez-García, Y.F. Tang, and L. Vázquez, Phys. Lett. A **236**, 314 (1997).

[42] D. J. Frantzeskakis, G. Theocharis, F. K. Diakonos, P. Schmelcher, and Yu. S. Kivshar, Phys. Rev. A **66**, 053608 (2002).

[43] N. Bilas and N. Pavloff, Phys. Rev. A **72**, 033618 (2005); Phys. Rev. Lett. **95**, 130403 (2005).

[44] G. Herring, P. G. Kevrekidis, R. Carretero-González, B. A. Malomed, D. J. Frantzeskakis, and A. R. Bishop, Phys. Lett. A **345**, 144 (2005).

[45] F. Tsitoura, Z. A. Anastassi, J. L. Marzuola, P. G. Kevrekidis, and D. J. Frantzeskakis, arXiv:1509.05206 (2015).

[46] V. Achilleos, P. G. Kevrekidis, V. M. Rothos, and D. J. Frantzeskakis, Phys. Rev. A **84**, 053626 (2011).

[47] A. Álvarez, J. Cuevas, F. R. Romero, C. Hamner, J. J. Chang, P. Engels, P. G. Kevrekidis, and D. J. Frantzeskakis, J. Phys. B **46**, 065302 (2013).

[48] J.-K. Xue, J. Phys. B **38**, 671 (2005).

[49] M. C. Davis, R. Carretero-González, Z. Shi, K. J. H. Law, P. G. Kevrekidis, and B. P. Anderson, Phys. Rev. A **80**, 023604 (2009).

[50] M. Ma, R. Carretero-González, P. G. Kevrekidis, D. J. Frantzeskakis, and B. A. Malomed, Phys. Rev. A **82**, 023621 (2010).

[51] W. Wang, P. G. Kevrekidis, R. Carretero-González, D. J. Frantzeskakis, T.J. Kaper, and M. Ma Phys. Rev. A **92**, 033611 (2015).

[52] P.G. Kevrekidis, D.J. Frantzeskakis, Reviews in Physics **1**, 140 (2016).

[53] J. Stockhofe, P.G. Kevrekidis, D.J. Frantzeskakis, P. Schmelcher, J. Phys. B: At. Mol. Opt. Phys. **44**, 191003 (2011).

[54] Y. S. Kivshar and X. Yang, Phys. Rev. E **49**, 1657 (1994).

[55] M.J. Ablowitz, B. Prinari and A.D. Trubatch, *Discrete and Continuous Nonlinear Schrödinger Systems*, Cambridge University Press (Cambridge, 2004).

[56] K. M. Mertes, J. W. Merrill, R. Carretero-González, D. J. Frantzeskakis, P. G. Kevrekidis, and D. S. Hall, Phys. Rev. Lett. **99**, 190402 (2007).

[57] C. Hamner, J. J. Chang, P. Engels, and M. A. Hoefer, Phys. Rev. Lett. **106**, 065302 (2011).

[58] M. A. Hoefer, C. Hamner, J. J. Chang, and P. Engels, Phys. Rev. A **84**, 041605 (2011).

[59] S. Middelkamp, J. J. Chang, C. Hamner, R. Carretero-González, P. G. Kevrekidis, V. Achilleos, D. J. Frantzeskakis, P. Schmelcher, and P. Engels, Phys. Lett. A **375**, 642 (2011).

[60] D. Yan, F. Tsitoura, P. G. Kevrekidis, and D. J. Frantzeskakis Phys. Rev. A **91**, 023619 (2015).

[61] P.G. Kevrekidis, H.E. Nistazakis, D.J. Frantzeskakis, B.A. Malomed, R. Carretero-González, Eur. Phys. J. D **28**, 181 (2004).

[62] H. Susanto, P. G. Kevrekidis, R. Carretero-González, B. A. Malomed, D. J. Frantzeskakis, and A. R. Bishop Phys. Rev. A **75**, 055601 (2007).

[63] I. Danaila, M.A. Khamehchi, V. Gokhroo, P. Engels, P.G. Kevrekidis, arXiv:1606.05607 (Phys. Rev. A, in press (2016)).

[64] B.A. Malomed, Prog. Opt. **43**, 71 (2002).

[65] M. Pola, J. Stockhofe, P. Schmelcher, and P. G. Kevrekidis Phys. Rev. A **86**, 053601 (2012).